LA-UR-14-20325
Approved for public release; distribution is unlimited.

Title: Effect of Beam Motion on Observed Image at Imaging Station C

Author(s): Schulze, Martin E.

Intended for: DARHT Technical Note

Issued: 2014-01-17

M. Schulze
16-December-2013

Effect of Beam Motion on Observed Image at Imaging Station C

Introduction

Imaging Station C on the DARHT II accelerator is used to measure beam spot sizes. Solenoid scans are used to measure the spot sizes as a function of the solenoid current and infer the beam emittance. Beam motion is observed during the measurement window and can contribute to the measured spot size. The effect of beam motion on the observed images at Station C is examined in this note. The variation in the beam position during the kicked beam pulse contributes to the beam spot size as measured at Station C. The beam motion is primarily in the vertical plane and is due to the kicker voltage rise time prior to the solenoid magnet. The effect of beam motion on the spot size is studied using LAMDA. From the measured beam position at BPM28 and BPM29 we determine the beam position and angle at the start of the LAMDA simulation. We then calculate the beam motion at Station C as a function of the S4 solenoid magnet current. The shot-to-shot variation in the beam motion is very small.

Initial Conditions

The S4 solenoid scan performed on 10/15-16/13 resulted in the preliminary results given in Table 1 below. The LAMDA fit assumed a beam energy and current of 16.5 MeV and 1.61 kA respectively. The starting point was located 177.9 cm upstream of the center of S4. Figure 1 shows a comparison of the measurements and the LAMDA fit for the envelope radius. The “best” fit was obtained for the beam parameters presented in Table 1. The beam position and angle at this starting point were determined from BPM28 and BPM29 data from shot 23539 corresponding to a S4 current of 0 A. Figures 2 and 3 show the time dependence of the position and angle in the horizontal and vertical planes respectively at the start of the LAMDA simulation.

Table 1: Results of LAMDA fit

Parameter	Value
Envelope Radius	1.07 cm
Envelope Angle	2.75 mrad
Normalized Emittance	720 π(mm-mrad)

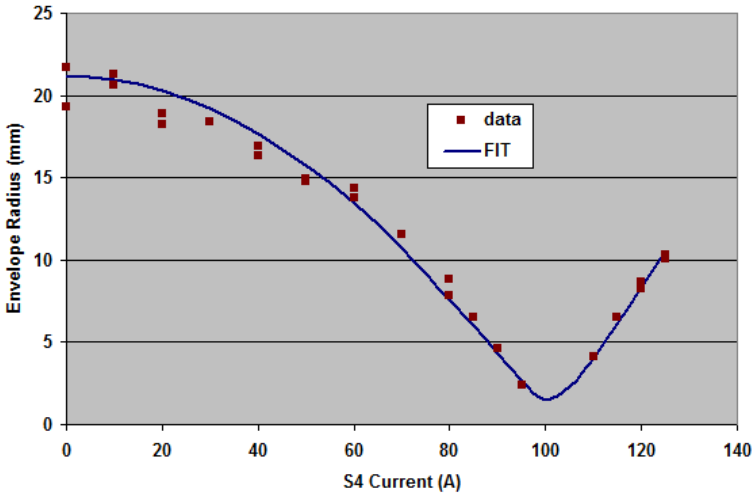

Figure 1: LAMDA fit and data

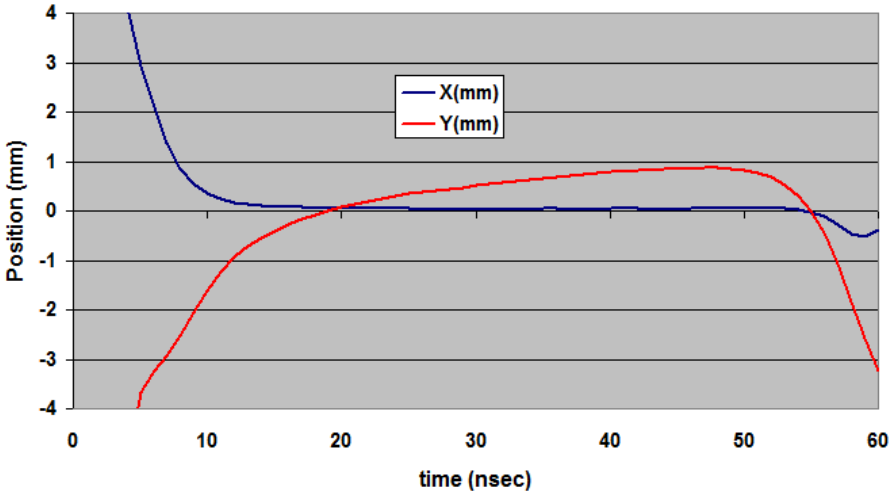

Figure 2: Time dependence of the horizontal and vertical position at the start of the LAMDA simulation calculated from shot 23539

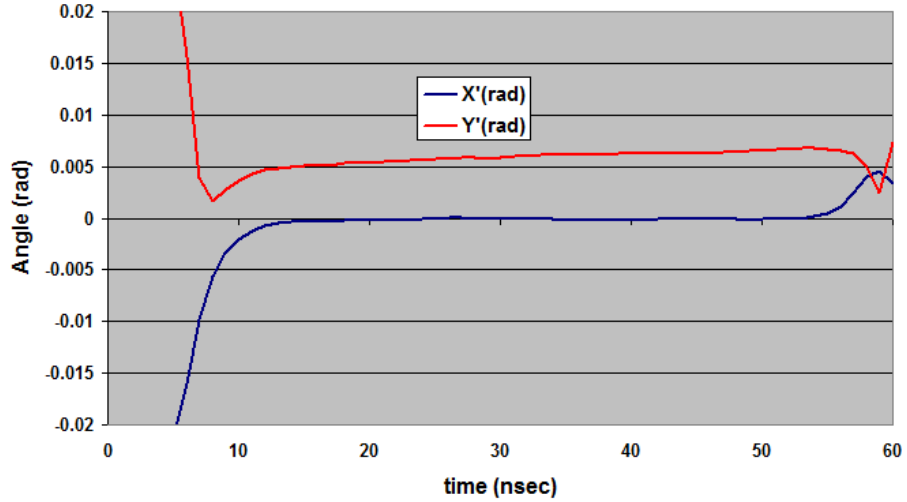

Figure 3: Time dependence of the horizontal and vertical angle at the start of the LAMDA simulation calculated from shot 23539

LAMDA Simulation

Using the above initial conditions, the beam motion at BPM29 was calculated for a few values of the S4 current as a check on the model. Figure 4 and 5 show the results of the LAMBDA simulation and measured beam position at BPM29 for an S4 current of 0 A. There is excellent agreement between the model and the data as expected since the data was used to provide the input conditions to the model. Figures 6 and 7 show the results with a S4 current of 100 A. To obtain agreement with the data it was necessary to use the exchange the horizontal and vertical input data presented in Figures 2 and 3. This is due to the fact that the bend plane to the septum dump was chosen to be the x axis. A comparison of Figures 6 and 7 shows excellent agreement. The same is true for a S4 current of 140 A as seen in Figures 8 and 9. The measured beam positions in Figures 5, 7 and 9 have been shifted for comparison with the LAMNDA simulation to account for steering and alignment uncertainties. The key feature in the LAMDA fit is that the scale and shape of the beam motion is in agreement with the BPM data.

Using the above initial conditions, the beam motion at Station C was calculated as a function of S4 current. Figures 10-13 show the predicted beam motion over the kicked pulse at Station for S4 currents of 0, 50, 100 and 140 A. The camera had a 10 nsec gate corresponding to a start time of about 25 ns in the LAMDA simulations. This corresponds to a start time of 2.765 in Figures 2 and 3. The time dependence of the beam motion is mostly linear over this time window as seen in Figures 10-13.

The beam motion over a 10 ns gate is presented in Figures 14 and 15 as a function of S4 current for two different time windows corresponding to 20-30 ns and 30-40 ns respectively. The beam motion is significantly smaller for the later gate. This is expected since the beam motion is dominated by the rise time of the kicker pulse. Figures 16 and 17 present this same beam motion as a percentage of the beam standard deviation as presented in Figure 1.

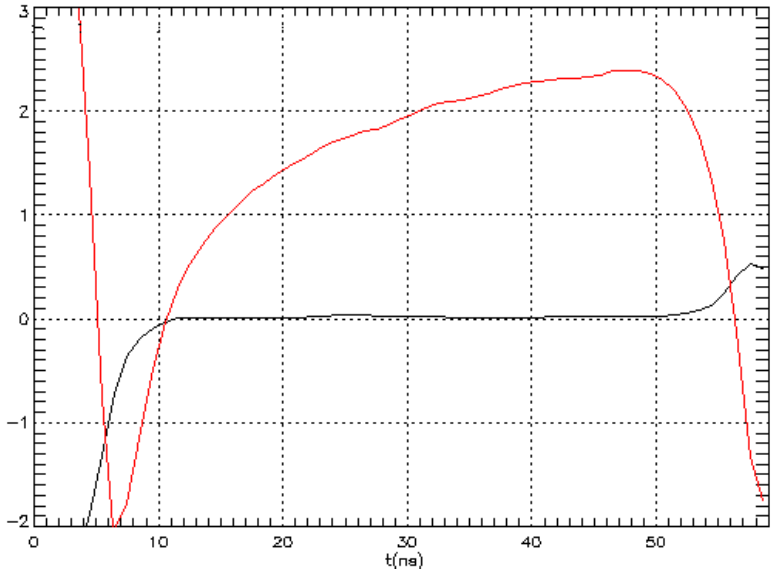

Figure 4: LAMDA Simulation for S4 = 0A at BPM29 (dimensions in cm) with horizontal (black) and vertical (red) beam position.

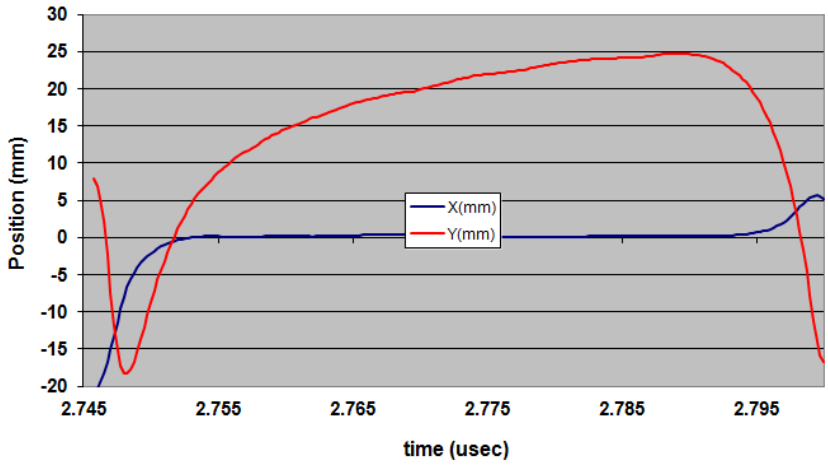

Figure 5: BPM29 data for S4=0 A

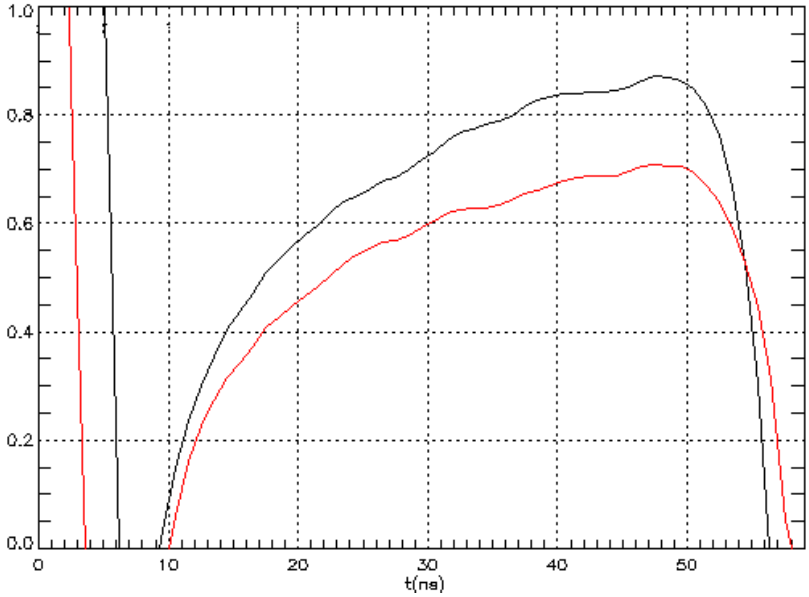

Figure 6: LAMDA Simulation for S4 = 100A at BPM29 (dimensions in cm) with horizontal (black) and vertical (red) beam position.

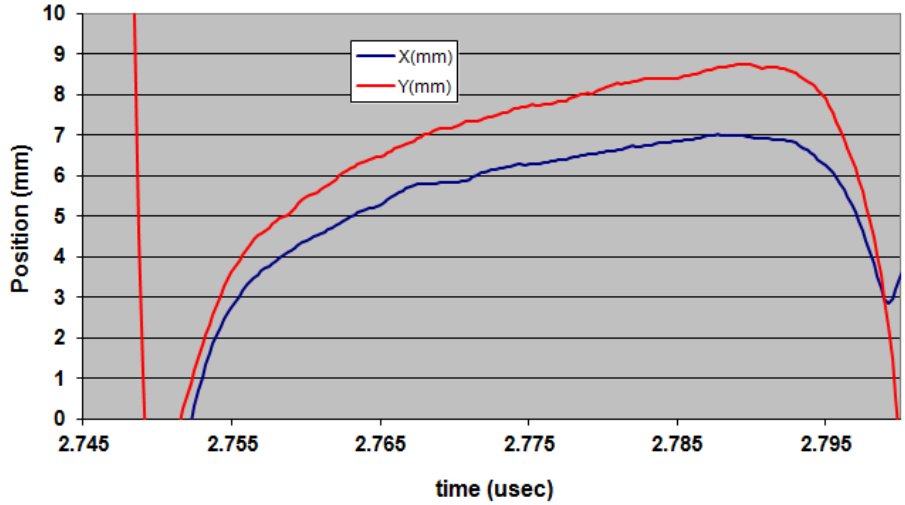

Figure 7: BPM29 data for S4=100 A

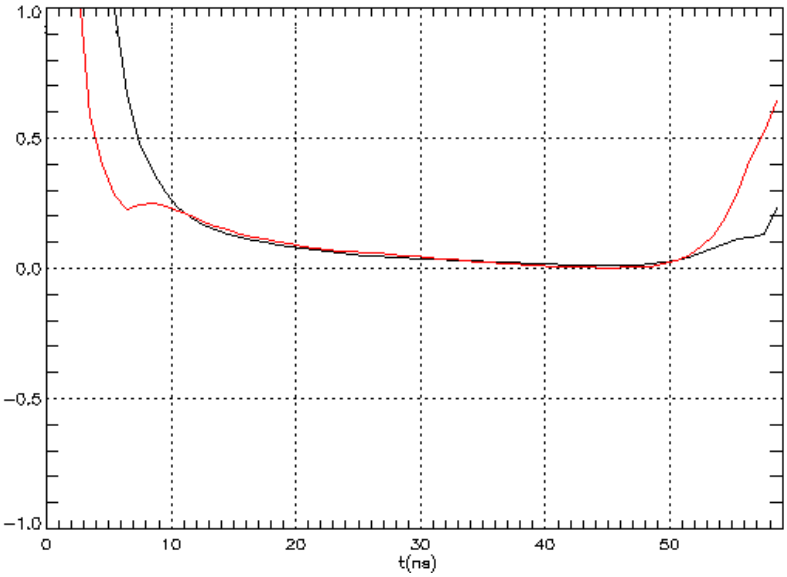

Figure 8: LAMDA Simulation for S4 = 140A at BPM29 (dimensions in cm) with horizontal (black) and vertical (red) beam position.

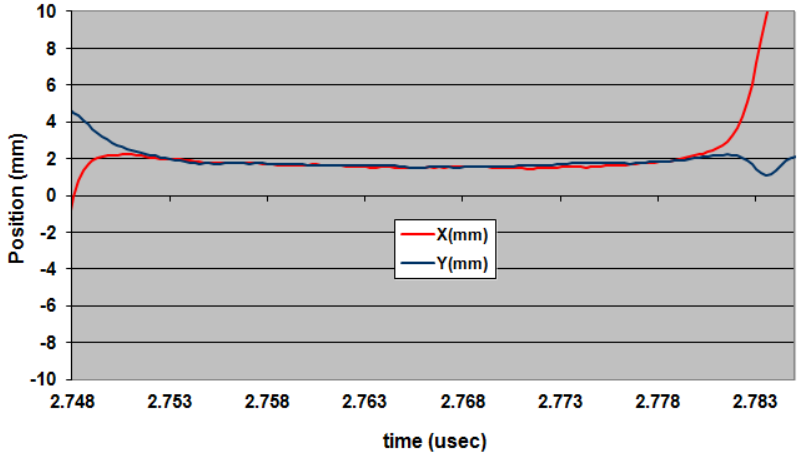

Figure 9: BPM29 data for S4=100 A

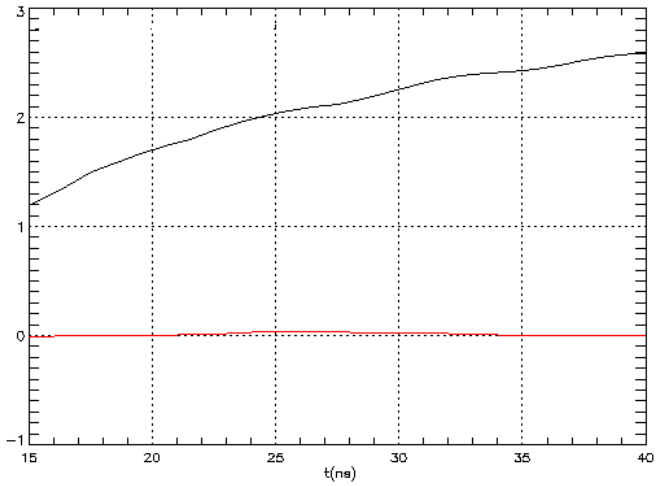

Figure 10: Horizontal (black) and vertical (red) beam motion in cm at Station C for S4 = 0 A.

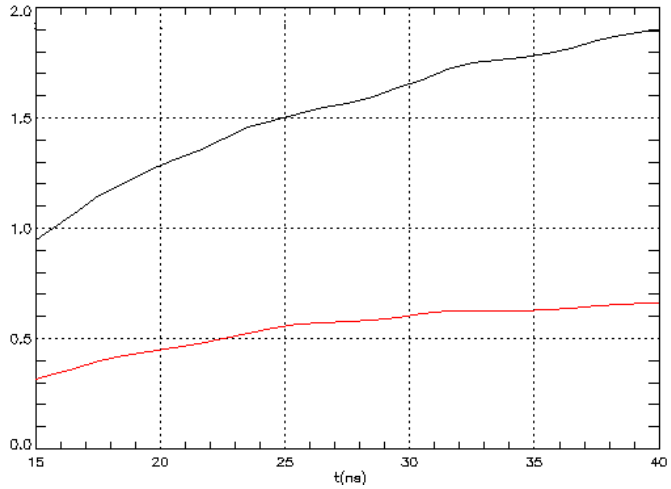

Figure 11: Horizontal (black) and vertical (red) beam motion in cm at Station C for S4 = 50 A.

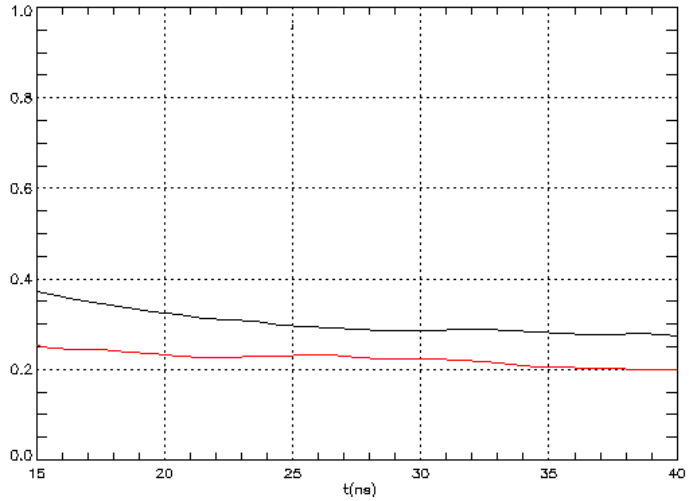

Figure 12: Horizontal (black) and vertical (red) beam motion in cm at Station C for S4 = 100 A.

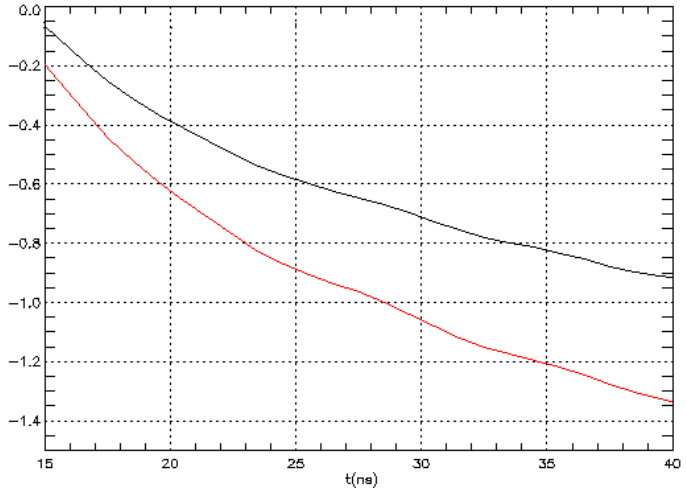

Figure 13: Horizontal (black) and vertical (red) beam motion in cm at Station C for S4 = 140 A.

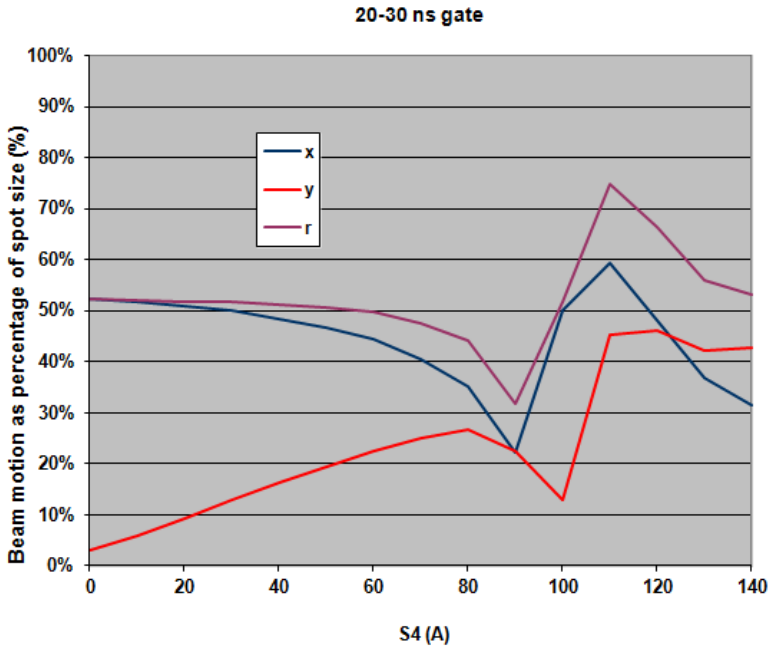

Figure 14: Horizontal and vertical beam motion in 10 ns camera gate from 20-30 ns as a function of the S4 current

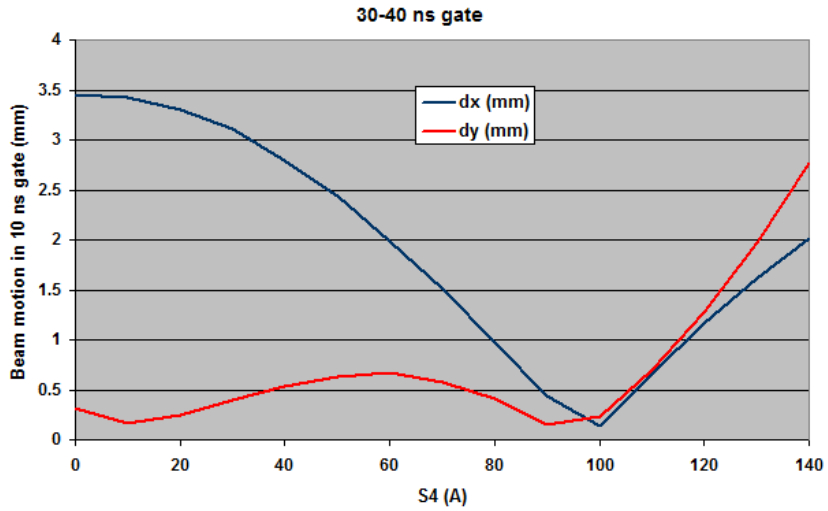

Figure 15: Horizontal and vertical beam motion in 10 ns camera gate from 30-40 ns as a function of the S4 current

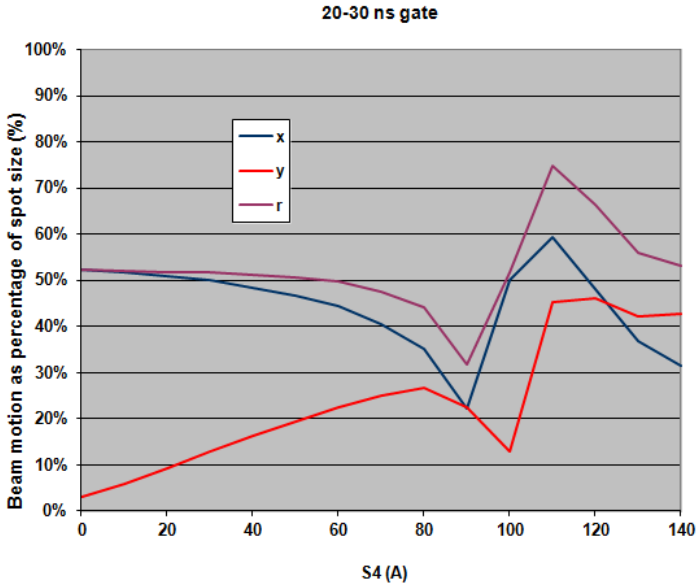

Figure 16: Beam motion as a percentage of the rms beam size for data presented in Figure 1 for 20-30 ns gate time

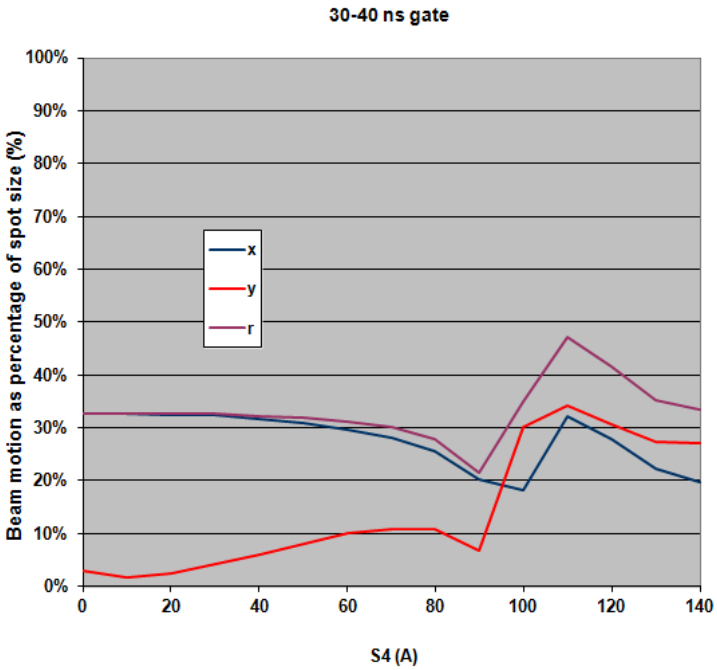

Figure 17: Beam motion as a percentage of the rms beam size for data presented in Figure 1 for 30-40 ns gate time

Change in spot size and shape due to beam motion

The LAMDA simulation provides a measure of the beam motion over the camera gate. Assuming the beam profile is Gaussian, we can write the following equation for the beam shape as a function of time.

$$F(x,y,t) = \frac{e^{\frac{-(x-u(t))^2}{2\sigma^2}} e^{\frac{-(y-v(t))^2}{2\sigma^2}}}{\sigma\sqrt{2\pi}} \quad (1)$$

The functions μ(t) and υ(t) represent the beam motion in x and y as a function of time respectively. To a good approximation, the functions μ(t) and υ(t) are linear functions of time and can be written as shown in the equations below. Note that the horizontal and vertical beam motion is coupled and υ(t) can be rewritten as a function of x.

$$\mu(t) = at + b \quad (2)$$

$$v(t) = a_y t + b_y = \alpha\mu(t) + \beta \quad (3)$$

Expanding the exponential term in Eq. 1 and using Eq. 3 for υ(t) we obtain:

$$\frac{-x^2-y^2+2(x\mu(t)+y\alpha\mu(t)+y\beta)-\mu(t)^2-\alpha^2u(t)^2-2\alpha\beta\mu(t)-\beta^2}{2\sigma^2} \quad (4)$$

We can write Eq. 4 in the following form:

$$\frac{-x^2-y^2-ft^2-gt-h}{2\sigma^2} \quad (5)$$

where,

$$f = a^2(1+\alpha^2) \tag{6}$$

$$g = 2(ab + \alpha^2 ab + \alpha\beta a - xa - y\alpha a) \tag{7}$$

$$h = (b^2 + \beta^2 + \alpha^2 b^2 + 2\alpha\beta b - 2y\alpha b - 2xb - 2y\beta) \tag{8}$$

We integrate F(x,y,t) over time of the camera gate to determine the resulting distribution. We can neglect all constant terms since we are not concerned about the normalization. Thus,

$$\int_{t_1}^{t_2} F(x,y,t)dt = C\, e^{\frac{-(x^2+y^2-2xb-2y\alpha b-2y\beta)}{2\sigma^2}} \int_{t_1}^{t_2} e^{\frac{-(ft^2+gt)}{2\sigma^2}} dt \tag{9}$$

An indefinite integral of this type can be determined as presented in Eq. 10 below.

$$\int \frac{1}{\sigma\sqrt{2\pi}} e^{-\frac{1}{2}\left(\frac{x-\mu}{\sigma}\right)^2} \mathrm{d}x = \frac{1}{2}\left(\operatorname{erf} \frac{x-\mu}{\sigma\sqrt{2}}\right) \tag{10}$$

Thus we determine the values of a_1, a_2 and a_3 from following equation.

$$ft^2 + gt = (a_1 t + a_2)^2 + a_3 \tag{11}$$

We obtain:

$$a_1 = \sqrt{f} \tag{12}$$

$$a_2 = {}^{g}\!\Big/\!_{2\sqrt{f}} \tag{13}$$

$$a_3 = -{}^{g^2}\!\Big/\!_{4f} \tag{14}$$

Rewriting Eq. 9 we obtain:

$$\int_{t_1}^{t_2} F(x,y,t)dt = C\, e^{\frac{-(x^2+y^2-2xb-2y\alpha b-2y\beta)}{2\sigma^2}} e^{\frac{g^2}{8f\sigma^2}} \int_{t_1}^{t_2} e^{\frac{-(a_1 t+a_2)^2}{2\sigma^2}} dt \tag{15}$$

Letting $\tau = a_1 t$, we obtain (again neglecting the overall normalization):

$$\int_{t_1}^{t_2} F(x,y,t)dt = e^{\frac{-(x^2+y^2-2xb-2y\alpha b-2y\beta)}{2\sigma^2}} e^{\frac{g^2}{8f\sigma^2}} \int_{a_1 t_1}^{a_1 t_2} e^{\frac{-(\tau+a_2)^2}{2\sigma^2}} d\tau \tag{16}$$

Using Eq. 9, we obtain:

$$\int_{t_1}^{t_2} F(x,y,t)dt = e^{\frac{-(x^2+y^2-2xb-2y\alpha b-2y\beta)}{2\sigma^2}} e^{\frac{g^2}{8f\sigma^2}} \left[erf\left(\frac{a_1 t_2 + a_2}{\sigma\sqrt{2}}\right) - erf\left(\frac{a_1 t_1 + a_2}{\sigma\sqrt{2}}\right)\right] \tag{17}$$

An approximation to the error function, erf(x), is given in Eq. 18 for x>0. The maximum error in this approximation is .0005. Note that the error function is an odd function so that erf(x)=-erf(-x).

$$\operatorname{erf}(x) \approx 1 - \frac{1}{(1 + a_1 x + a_2 x^2 + a_3 x^3 + a_4 x^4)^4}$$

$$where\ a_1 = 0.278393, a_2 = 0.230389, a_3 = 0.000972, a_4 = 0.078108 \tag{18}$$

Analysis

The beam motion is predicted at Station C as shown in Figures 10-13. The linear fit to the beam motion is then calculated between the 25-35 nsec time window corresponding to the camera gate to determine a, b, α and β. The beam distribution is then integrated over this time window and compared to the beam distribution without beam motion. The results are presented below for selected S4 currents.

The fit to the beam motion predicted by LAMDA for S4 = 0 A is shown in Figure 18. Figure 19 compares the corresponding beam distributions (x and y) projected onto the orthogonal axes. The projected beam distributions without beam motion (xg and yg) are also shown for comparison. The beam motion has very little effect on the projected beam distribution as seen in Figure 19. Similar results are shown for S4 = 100 A in Figures 20 and 21. Again no appreciable change to the beam size as a result of beam motion is observed. The analysis for a S4 current of 120 and 140 are presented in Figures 22 and 23 respectively also shows no appreciable increase in the beam size. Based on these results and the ratio of the beam size to the standard deviation presented in Figures 16 and 17, similar results are expected for all values of the S4 current.

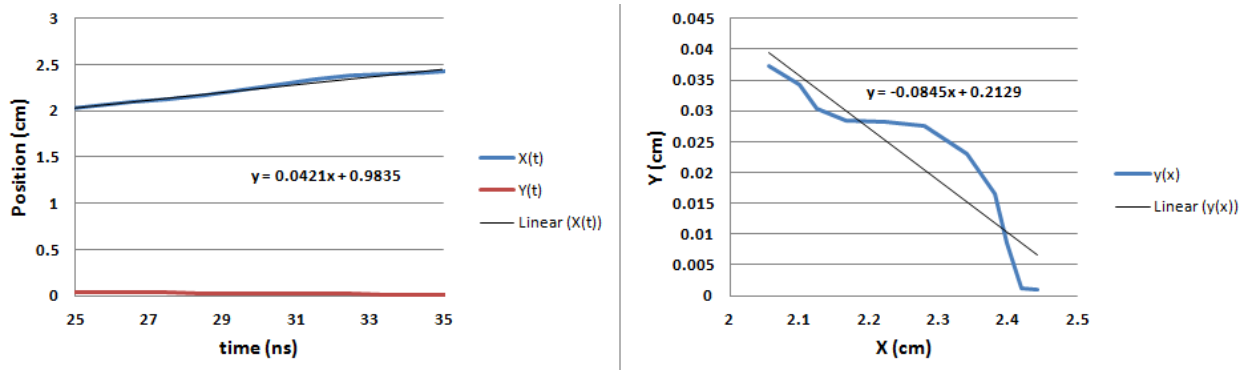

Figure 18: Beam motion for S4 = 0 A. The figure on the left shows x(t) and y(t) with a linear fit to x(t). The figure on the right shows a plot of y(x) and a corresponding linear fit.

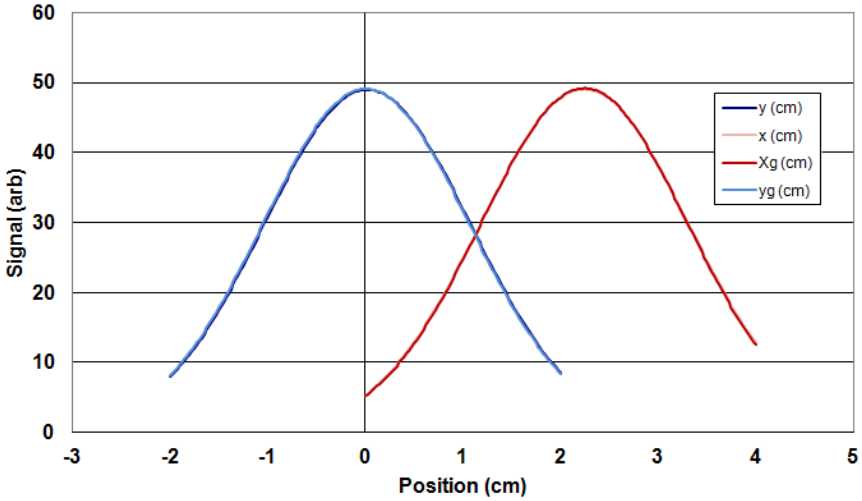

Figure 19: Beam distributions projected onto the two orthogonal axes with and without beam motion at S4 = 0 A.

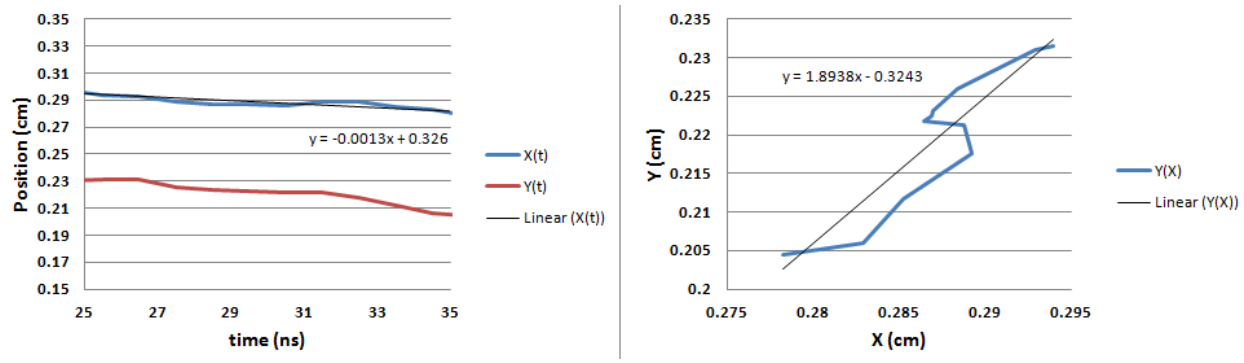

Figure 20: Beam motion for S4 = 100 A. The figure on the left shows x(t) and y(t) with a linear fit to x(t). The figure on the right shows a plot of y(x) and a corresponding linear fit.

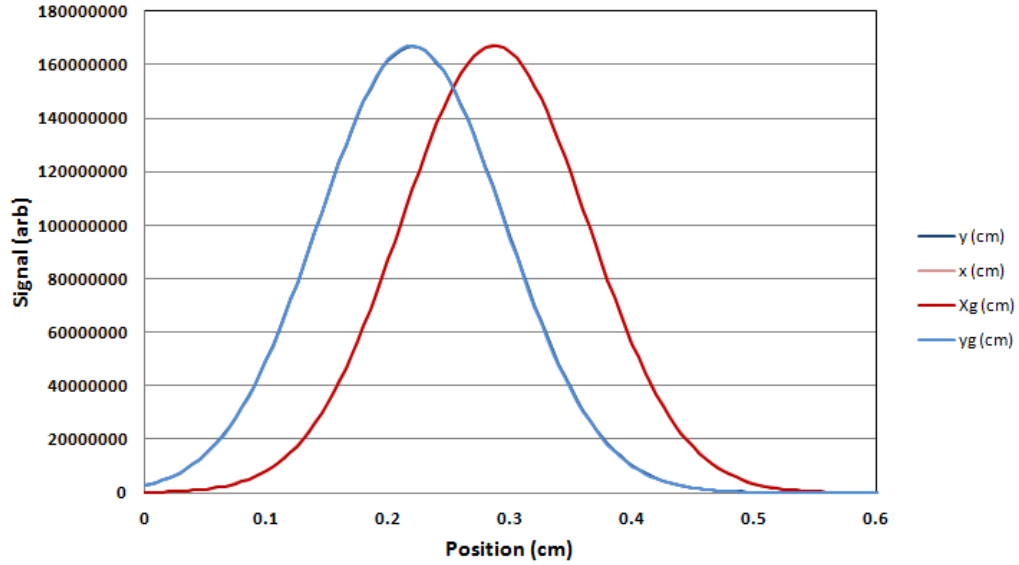

Figure 21: Beam distributions projected onto the two orthogonal axes with and without beam motion at S4 = 100 A.

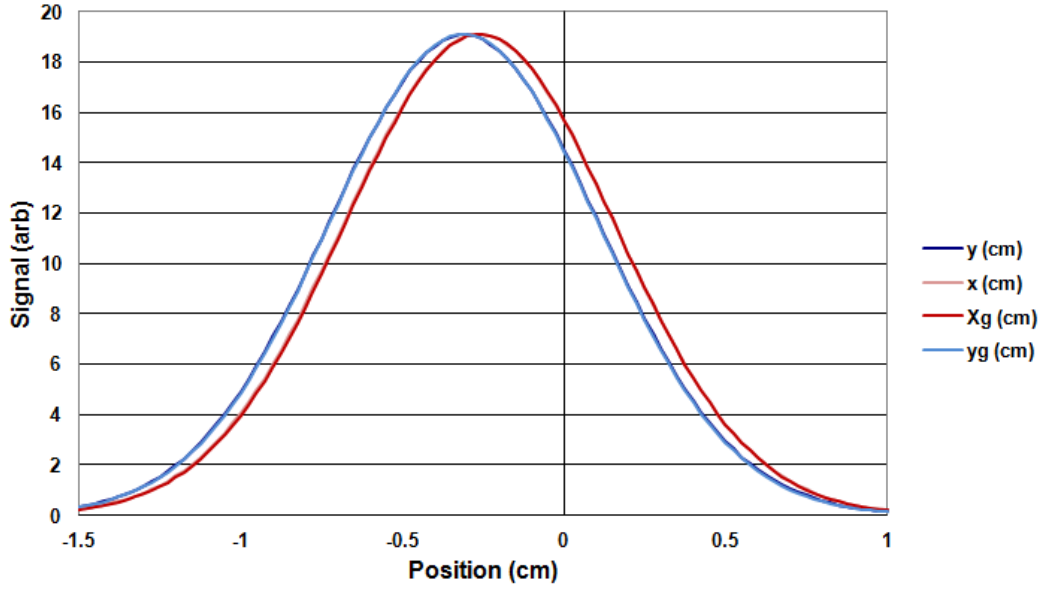

Figure 22: Beam distributions projected onto the two orthogonal axes with and without beam motion at S4 = 120 A.

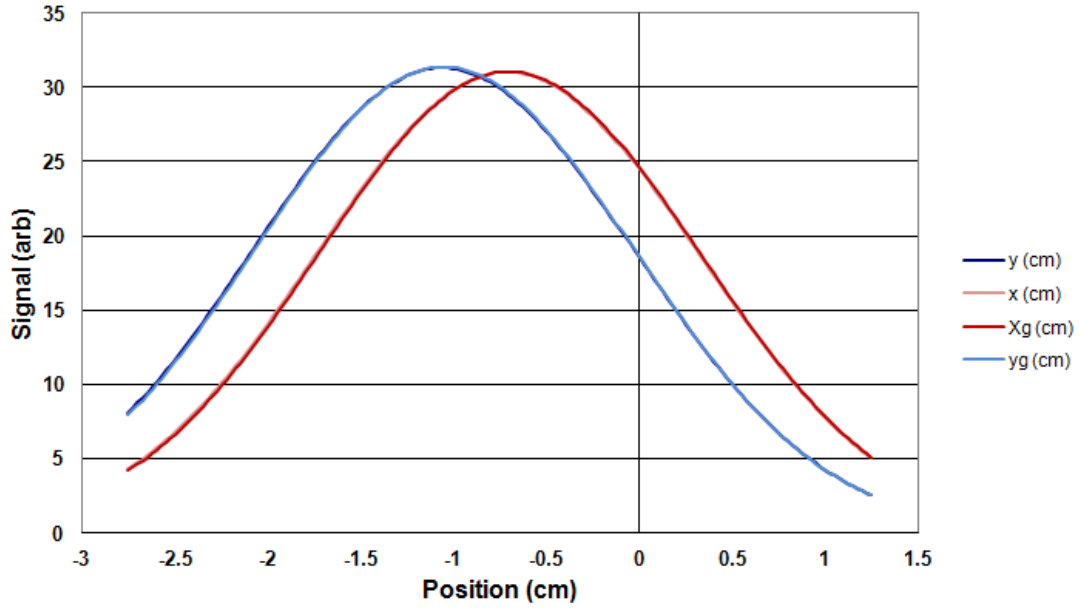

Figure 23: Beam distributions projected onto the two orthogonal axes with and without beam motion at S4 = 140 A.

Discussion and Conclusion

In order to validate the results of the prior section, a study was performed in which 1D Gaussian distributions with evenly spaced centroids are summed and compared. An example is shown in Figure 24. There are 20 black curves with σ=0.5 with varying centroids from -.25 to .25 or 1σ. Here the red curve is the sum of the black curves scaled to the same amplitude of a single black curve. The resulting red curve has a standard deviation that is very close to the individual black curves. By varying the ration of the motion to the standard deviation, the contribution of the beam motion to the observed spot size can be quantified. Figure 25 shows the case for a beam motion of $\delta x = .25\sigma$. Three curves are plotted as defined below:

1. **Single** Gaussian with σ=1
2. **Sum** of 51 Gaussians with evenly space centroids between $-\delta x/2$ and $\delta x/2$
3. A least squares **fit** to the sum assuming a Gaussian with a different standard deviation

All curves are scaled to the same amplitude. In this case the three curves are essentially the same to within a line width. Figure 26 show the case with $\delta x=\sigma$. There is a small but distinct broadening of the distribution. Note that the sum of the Gaussians is essentially identical to a Gaussian with a different standard deviation. Figure 27 show the case with $\delta x=2\sigma$. Here the broadening of the spot is much greater and there is a small but distinct difference between the sum and a Gaussian. Repeating this analysis to many values of δx, the increase in spot size as a function of the beam motion can be determined as presented in Figure 28. The curve can be fit to a quadratic polynomial with the intercept set to 0 as shown in Figure 28.

This analysis can be readily extended to 2D. Consider a 2D spot in which the beam motion is confined to a single axis. In this case, assigning a single standard deviation to the distribution would result in an increase of the beam size by a factor of two less than that presented in Figure 28.
Comparing Figure 28 to the beam motion predicted in Figure 16 implies that the gate time can be moved earlier in the kicked pulse which should help mitigate ion effects that distort the beam size. Using the measured beam motion as determined from the LAMDA simulation and the formula in Figure 28, the overall increase in the spot size as a function of S4 current is plotted in Figure 29 for two gate intervals. The resulting increase in spot size is less than 1% for the window from 25-35 ns. Note that the results of this analysis are very dependent on the tune of the five quadrupole magnets located between the kicker and Station C. The sensitivity to the overall machine tune is much less due to the small amount of beam motion over the measurement window except for that introduced by the kicker.

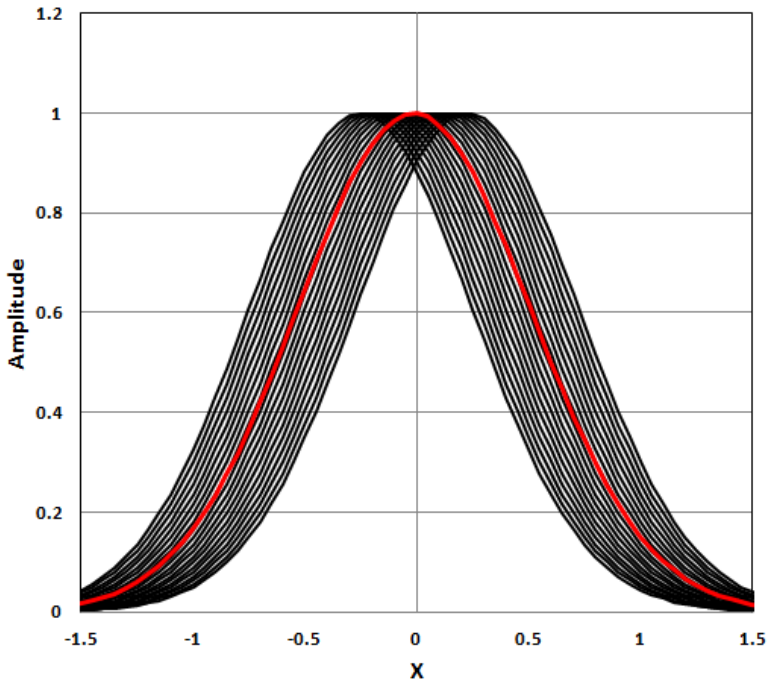

Figure 24: Comparison of sum of 20 individual Gaussian distributions (black) and sum of the distributions (red).

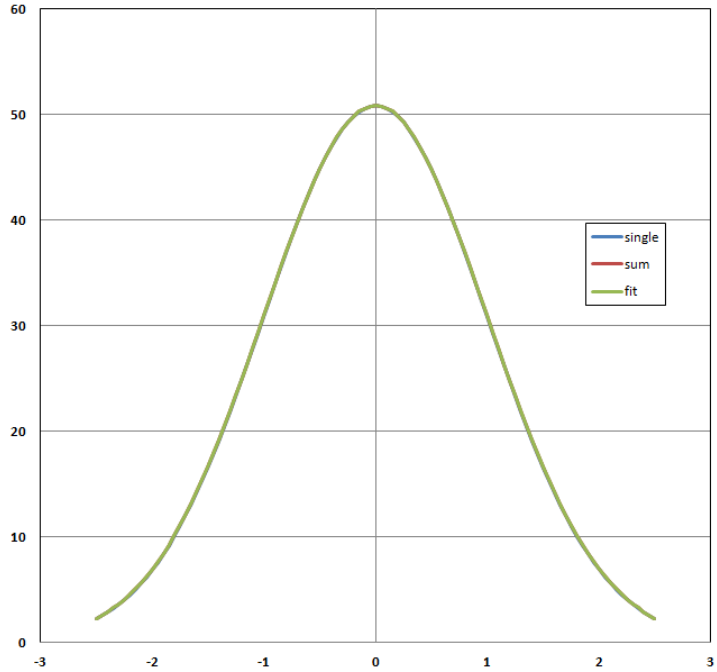

Figure 25: Effect of beam motion with $\delta x=.25\sigma$ and $\sigma=1$

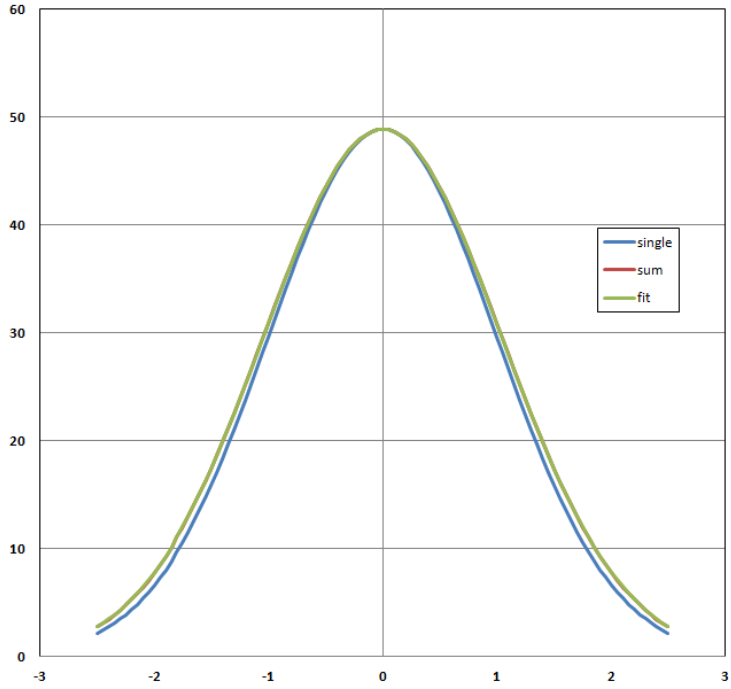

Figure 26: Effect of beam motion with $\delta x=\sigma$ and $\sigma=1$

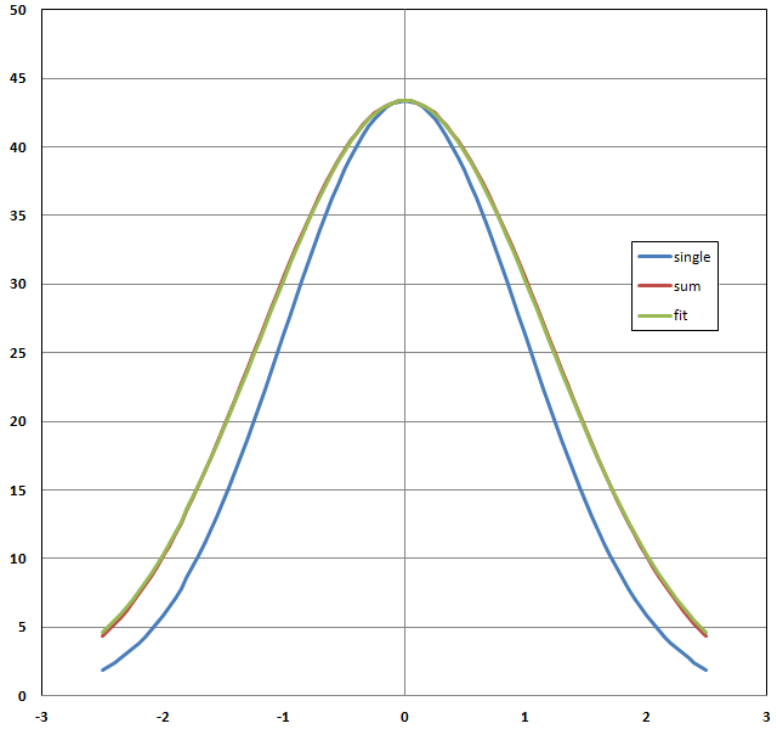

Figure 27: Effect of beam motion with $\delta x=2\sigma$ and $\sigma=1$

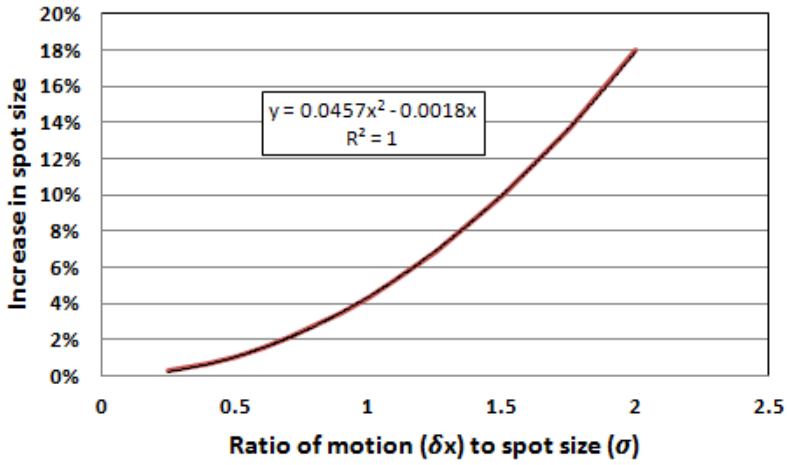

Figure 28: Relative contribution of beam motion to spot size.

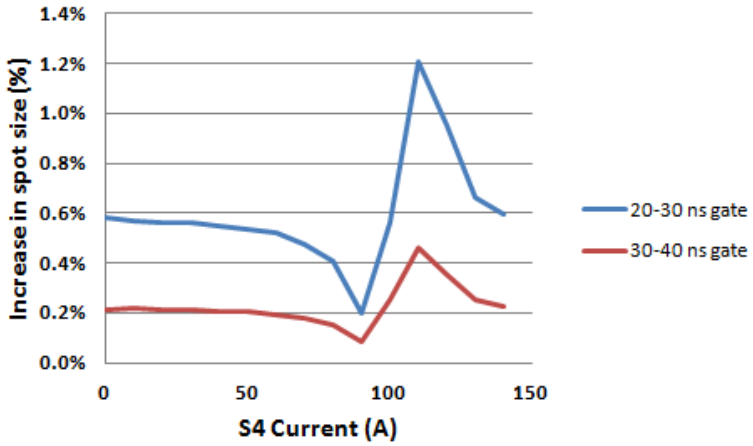

Figure 29: Percentage increase in the spot size as a function of the S4 current for the measured beam motion as inferred from LAMDA simulation